Paleoceanography and Paleoclimatology

RESEARCH ARTICLE
10.1029/2021PA004281

Little Change in Ice Age Water Mass Structure From Cape Basin Benthic Neodymium and Carbon Isotopes

Sophia K. V. Hines[1,2], Louise Bolge[1], Steven L. Goldstein[1,3], Christopher D. Charles[4], Ian R. Hall[5], and Sidney R. Hemming[1,3]

[1]Lamont-Doherty Earth Observatory of Columbia University, Palisades, NY, USA, [2]Department of Marine Chemistry & Geochemistry, Woods Hole Oceanographic Institution, Woods Hole, MA, USA, [3]Department of Earth and Environmental Sciences, Columbia University, Palisades, NY, USA, [4]Scripps Institution of Oceanography, UC San Diego, La Jolla, CA, USA, [5]School of Earth and Environmental Sciences, Cardiff University, Cardiff, UK

Key Points:

- We present high-resolution, co-registered εNd, $\delta^{13}C$, and $\delta^{18}O$ records from the last 160,000 years
- Compiled Cape Basin εNd data show maximum North Atlantic Deep Water (NADW) influence at 2,615 m across the last glacial cycle
- The data does not favor significant shoaling of the core depth of NADW during the Last Glacial Maximum, but there is enhanced deep stratification

Supporting Information:

Supporting Information may be found in the online version of this article.

Correspondence to:

S. K. V. Hines,
shines@whoi.edu

Citation:

Hines, S. K. V., Bolge, L., Goldstein, S. L., Charles, C. D., Hall, I. R., & Hemming, S. R. (2021). Little change in ice age water mass structure from Cape Basin benthic neodymium and carbon isotopes. *Paleoceanography and Paleoclimatology*, *36*, e2021PA004281. https://doi.org/10.1029/2021PA004281

Received 13 APR 2021
Accepted 11 OCT 2021

Abstract A common conception of the deep ocean during ice age episodes is that the upper circulation cell in the Atlantic was shoaled at the Last Glacial Maximum compared to today, and that this configuration facilitated enhanced carbon storage in the deep ocean, contributing to glacial CO_2 draw-down. Here, we test this notion in the far South Atlantic, investigating changes in glacial circulation structure using paired neodymium and benthic carbon isotope measurements from International Ocean Discovery Program Site U1479, at 2,615 m water depth in the Cape Basin. We infer changes in circulation structure across the last glacial cycle by aligning our site with other existing carbon and neodymium isotope records from the Cape Basin, examining vertical isotope gradients, while determining the relative timing of inferred circulation changes at different depths. We find that Site U1479 had the most negative neodymium isotopic composition across the last glacial cycle among the analyzed sites, indicating that this depth was most strongly influenced by North Atlantic Deep Water (NADW) in both interglacial and glacial intervals. This observation precludes a hypothesized dramatic shoaling of NADW above ~2,000 m. Our evidence, however, indicates greater stratification between mid-depth and abyssal sites throughout the last glacial cycle, conditions that developed in Marine Isotope Stage 5. These conditions still may have contributed to glacial carbon storage in the deep ocean, despite little change in the mid-depth ocean structure.

1. Introduction

The modern global ocean overturning circulation has a "figure-eight" structure (Talley, 2013). Deep water formed in the North Atlantic (North Atlantic Deep Water; NADW) is sufficiently dense that it upwells in a region of the Southern Ocean where surface flow is southward, and it therefore becomes a source for newly forming Antarctic Bottom Water (AABW). Antarctic Bottom Water is the densest water in the ocean, and it flows northward into the deep Atlantic, Pacific, and Indian ocean basins. The portion of AABW that flows into the Atlantic Ocean diffusively upwells into NADW and returns to the Southern Ocean. It is only after flowing into the Pacific or Indian Oceans that AABW can diffusively mix to form water masses (Pacific or Indian Deep Water; PDW/IDW) that are sufficiently low density such that they upwell in a region of the Southern Ocean where surface flow is northward, finally transforming into shallow Antarctic Intermediate Water (AAIW) that can close the circulation loop through northward flow in the Atlantic (Figure 2a) (Talley, 2013).

Some deep ocean tracers suggest that this ocean circulation was fundamentally different during the Last Glacial Maximum (LGM; ~22–18 ka), with a shoaled version of NADW, a "two-cell" circulation structure (Figure 2d), and increased stratification between the two cells (Adkins, 2013; Curry & Oppo, 2005; Ferrari et al., 2014; Lund et al., 2011). In this context, we define "shoaling" as an elevation in the depth of the main core of NADW and a reduction in the amount of NADW in the abyssal ocean. The two-cell circulation configuration has the potential to store more carbon in the deep ocean, particularly if the depth of the isopycnal separating the upper and lower circulation cells shoals above the depth of the mid-ocean ridges (~2,000 m) into a region with reduced vertical mixing; consequently, this altered deep ocean geometry is a commonly cited mechanism by which the ocean circulation contributed to glacial CO_2 draw-down. Much of the evidence for a two-cell LGM circulation structure comes from carbon isotope measurements recorded in

benthic foraminifera. Recently, however, some authors have re-examined the LGM circulation configuration by including additional paleo-circulation proxies, such as neodymium isotopes and the air-sea component of $\delta^{13}C$. While there are uncertainties and complications associated with most paleo proxies (Gu et al., 2020; Oppo et al., 2018), some of these recent studies have questioned the canonical shoaled LGM circulation, arguing instead that the glacial ocean had a similar structure to the modern, with very minor changes in the core depth of NADW (Gebbie, 2014; Howe et al., 2016; Oppo et al., 2018; Pöppelmeier et al., 2020) and significant amounts of NADW in the deep ocean (Howe et al., 2016; Pöppelmeier et al., 2020).

Carbon and neodymium isotope ratios are two commonly used paleoceanographic water mass proxies that have been used to examine ocean circulation structure at the LGM and across glacial cycles of the Late Pleistocene. Neodymium (Nd) isotope ratios have been described as "quasi-conservative" in the deep and intermediate ocean (Frank, 2002; Goldstein & Hemming, 2003, and references therein), meaning that they generally approximate water mass mixing within the global overturning circulation away from endmember source regions. Nd isotopic ratios in rocks of different ages vary due to the alpha-decay of ^{147}Sm to ^{143}Nd, with a half-life of 106 Ga, and the average Sm/Nd ratio experienced by the Nd over geologic time. The Nd isotopic composition of the major water mass endmembers is set by erosion and weathering of surrounding continents (with inputs at the surface and the sediment-water interface), which have different isotopic compositions that reflect the amount of time the Nd has been in the continental crust (Goldstein & O'Nions, 1981; Goldstein et al., 1984; Jeandel et al., 2007; Piepgras et al., 1979; Robinson et al., 2021; van de Flierdt et al., 2016). The Nd isotopic composition, εNd, is defined as $(R_{samp}/R_{CHUR} - 1) \times 10{,}000$, where R is $^{143}Nd/^{144}Nd$ and CHUR refers to "Chondritic Uniform Reservoir," a proxy for the modern bulk earth composition; this study uses a $^{143}Nd/^{144}Nd$ ratio of 0.512638 (Jacobsen & Wasserburg, 1980). Archean and Proterozoic terrains in northern Canada and Greenland have very negative εNd values, driving seawater in the North Atlantic toward negative values of −13 to −14 (Lambelet et al., 2016). Young volcanic rocks around the Pacific have positive εNd values, imparting less negative isotopic values of −3 to −4 to deep water in the Pacific (Amakawa et al., 2004, 2009; Behrens et al., 2018; Fröllje et al., 2016; Haley et al., 2014; Pahnke et al., 2012; Piepgras & Jacobsen, 1988; Shimizu et al., 1994; Vance et al., 2004; Wu, 2019; Zimmermann et al., 2009). Southern Ocean waters have intermediate εNd values of −8 to −11, largely reflecting mixing between the North Atlantic and North Pacific endmembers (Garcia-Solsona et al., 2014; Stichel et al., 2012).

Carbon isotopes are non-conservative, reflecting partitioning between organic and inorganic carbon phases. Biological production at the ocean surface leaves the $\delta^{13}C$ of inorganic carbon at higher values and remineralization in the subsurface drives the $\delta^{13}C$ of inorganic carbon to lower values (Eide et al., 2017). However, differences in source water and deep water formation mechanisms for northern (NADW) versus southern-sourced (AAIW/AABW) water masses lead to different $\delta^{13}C$ values upon formation, allowing this tracer to function as a paleo water mass proxy (e.g., Curry et al., 1988; Oppo & Fairbanks, 1987). NADW is sourced from low-latitude surface waters, which are fully depleted of nutrients (and therefore high in $\delta^{13}C$). In contrast, source waters for AAIW and AABW do not spend enough time at the surface for biological production to exhaust their nutrients, and, accordingly, these water masses form with much lower $\delta^{13}C$ than NADW. Over time, deep water $\delta^{13}C$ values decrease as organic matter from the surface is respired; furthermore, shifts in the intensity and location of gas exchange can impart a non-negligible "thermodynamic" stamp on interior ocean $\delta^{13}C$ values. Thus, $\delta^{13}C$ can be used to reconstruct the relative mixing fraction of northern and southern sourced waters only if one assumes similar deep water formation mechanisms in the past, relatively small changes in circulation rate, and minimal complications from gas exchange.

In the Cape Basin, Nd isotopes track mixing between NADW, which primarily enters the basin from the north across the Walvis Ridge, and Southern Ocean water masses (AABW, Upper and Lower Circumpolar Deep Water—U/LCDW, AAIW), which have larger mixing fractions of water derived from the Pacific (Arhan et al., 2003; Bower et al., 2019; Garzoli et al., 2015; Kersalé et al., 2019; Orsi et al., 1999; Stramma & England, 1999) (Figure 1b). Mixing analyses using Nd isotopes by Garcia-Solsona et al. (2014) and Rahlf et al. (2019) indicate that NADW mixes conservatively with circumpolar deep waters in this region.

In the modern Cape Basin, the core of NADW is located along the South African margin at around 2,500 m water depth, very close to the depth of Site U1479 (Figures 1b and 1c; marked in blue in Figure 2b). ODP Sites 1087 and 1088 (at 1,372 and 2,082 m, respectively) are also somewhat influenced by NADW, sitting just above the core of this water mass. Water returning from the Pacific Ocean (PDW) becomes UCDW upon

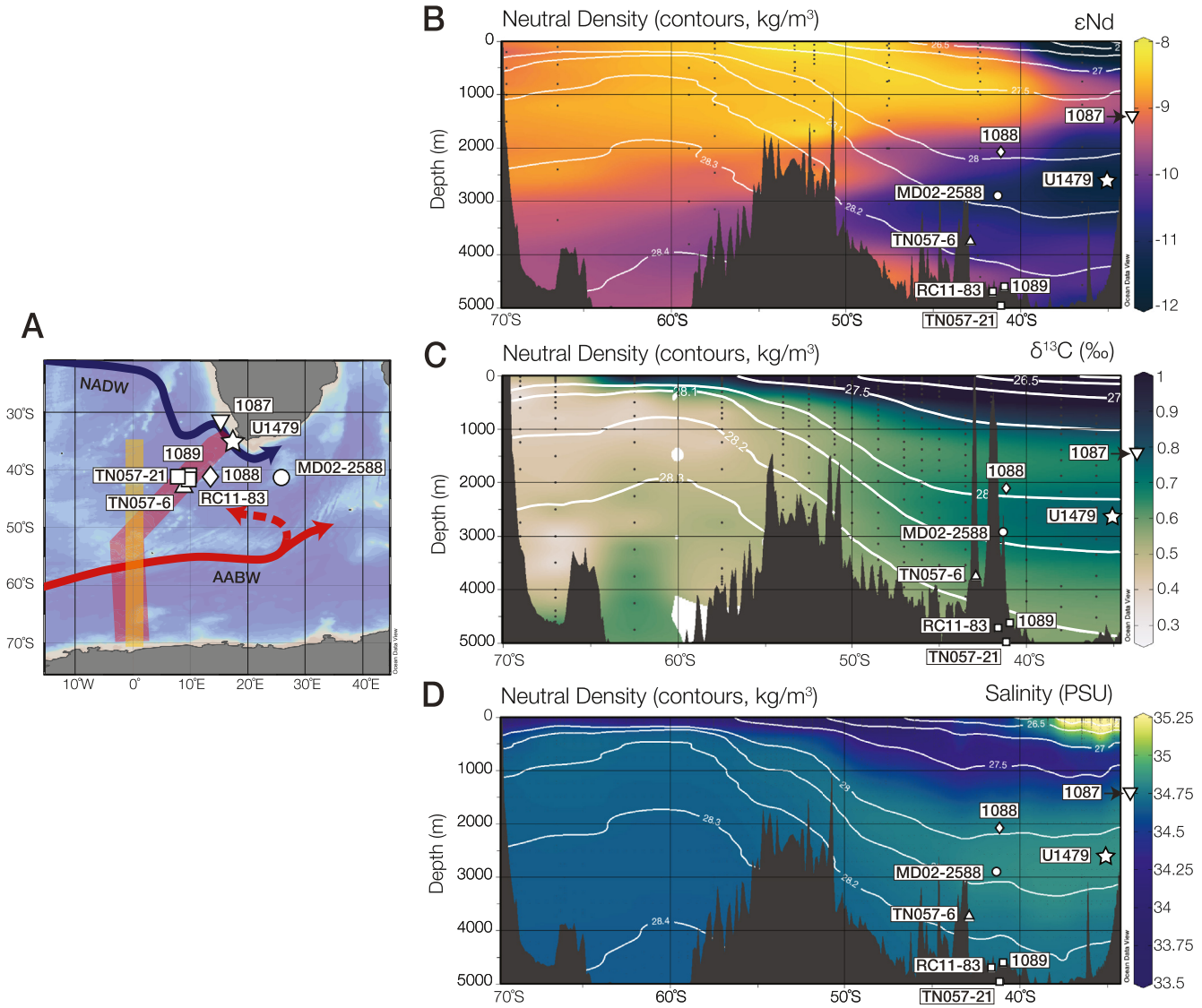

Figure 1. Modern hydrography of the Cape Basin. (a) Map of the Cape Basin with sections (red for εNd and salinity and orange for $\delta^{13}C$) and core locations marked (same symbols as b, c, and d). Idealized flow path of North Atlantic Deep Water and Antarctic Bottom Water also marked (blue and red, respectively). (b) εNd section from the BONUS GoodHope IPY-GEOTRACES cruise to the Southeast Atlantic (red in Panel a) (Garcia-Solsona et al., 2014), compiled in the GEOTRACES Intermediate Data Product (Schlitzer et al., 2018) with contours of Neutral Density in white. (c) $\delta^{13}C$ section (orange in Panel a) from GLODAPv2 (Olsen et al., 2016) with contours of Neutral Density in white. (d) Salinity section (red in Panel a) with contours of Neutral Density in white. Arrows next to the symbol for Site 1,087 in Panels b, c, and d indicate the depth of the core, which is slightly off the section. More detailed information for the cores is in Table 1. Figure was made using the Ocean Data View Software (Schlitzer, 2021).

entering the Southern Ocean, shallower and further to the south than NADW (marked in red in schematic Figure 2). The deepest sites in the Cape Basin (RC11-83 and TN057-21 at 4,718 and 4,981 m, respectively) are bathed in a mixture of AABW and LCDW (Figure 1). Therefore, in the modern Cape Basin, the vertical εNd structure recorded by cores 1087, 1088, U1479, RC11-83, and TN057-21 (Figure 2c) has intermediate εNd values at the shallowest sites (1087, 1088), the most negative εNd values at Site U1479, and the least negative values at the deep sites RC11-83 and TN057-21.

If the ocean had a "two-cell" circulation structure at the LGM (Figure 2d) (Adkins, 2013; Curry & Oppo, 2005; Ferrari et al., 2014; Lund et al., 2011), this hypothetical arrangement would likely switch the relative positions of NADW and UCDW in the LGM Cape Basin, converting them into glacial North Atlantic Intermediate Water (GNAIW) and Glacial Lower Circumpolar Deep Water (GLCDW), respectively (Figure 2e). This would increase the relative influence of NADW/GNAIW at the shallower Cape Basin sites

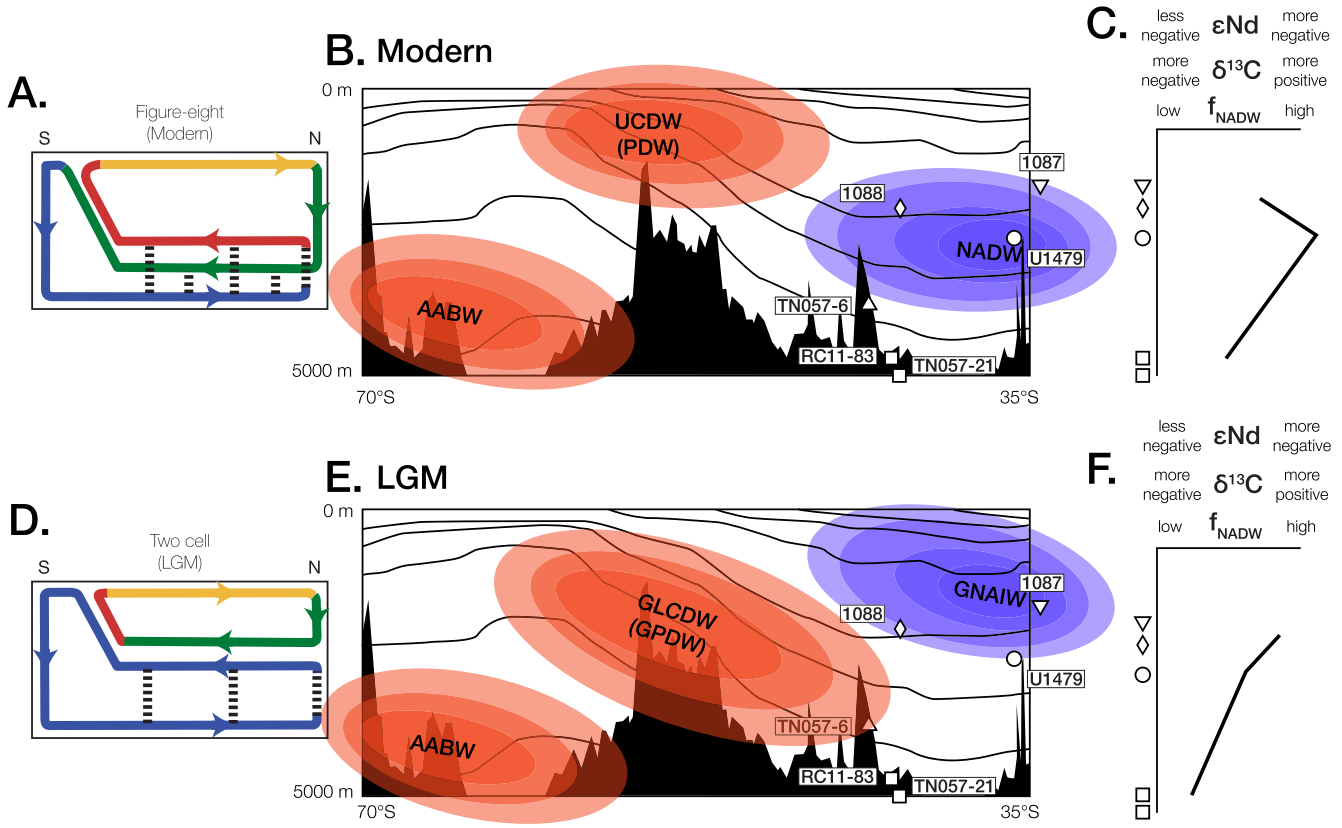

Figure 2. Hypothetical changes in εNd vertical structure in the Cape Basin between the Last Glacial Maximum (LGM) and Modern ocean. (a) Modern figure-eight ocean circulation structure schematic (adapted from Talley, 2013). Water masses represented are: North Atlantic Deep Water (NADW) (green), Antarctic Bottom Water (blue), Pacific or Indian Deep Water (red), and AAIW (yellow). (b) Schematic section through the Cape Basin (adapted from Figure 1) showing the relative positions of NADW (blue) and UCDW (red). (c) Schematic fraction of NADW (f_{NADW}) as a depth profile based on panel B, showing the positions of cores 1087, 1088, U1479, RC11-83 and TN057-21 (symbols corresponding to labeled section). (d) LGM two-cell ocean circulation schematic (adapted from Ferrari et al., 2014 and following the same color scheme as in Panel a). (e) Schematic section through the Cape Basin (as in Panel b) showing hypothesized relative positions of NADW (now glacial North Atlantic Intermediate Water, blue) and UCDW (now Glacial Lower Circumpolar Deep Water, red) at the LGM. (f) Schematic f_{NADW} depth profile through the Cape Basin at the LGM based on hypothetical water mass arrangement in panel (e).

(1087 and 1088) and reduce its influence at Site U1479. The hypothesized two-cell circulation also implies that the feed waters for the formation of AABW have a larger fraction of water returning from the Indo-Pacific (Figure 2d). This would change the LGM vertical εNd and $\delta^{13}C$ structure, such that Sites 1087 and 1088 record the most negative εNd values and most positive $\delta^{13}C$, followed by Site U1479, and sites RC11-83 and TN057-21 (Figure 2f).

In this paper, we use both neodymium and carbon isotopes in concert to assess the evidence for the canonical LGM "two-cell" circulation structure in the Cape Basin—in other words, testing the hypothesis posed in Figure 2. We take advantage of previously published εNd and $\delta^{13}C$ records from other depths in this area (Figure 1), and with the addition of our new record from International Ocean Discovery Program (IODP) Site U1479 in the core of modern NADW, we provide key constraints on water mass structure over the last glacial cycle.

2. Methods

2.1. Site Description

IODP Expedition 361 "Southern African Climates" cored six sites along the margin of southeastern Africa that trace the path of the Agulhas current system. Site U1479 is located in the Cape Basin on the slope of the Greater Agulhas Bank, beyond the modern Agulhas Retroflection and in the direct path of the Agulhas Leakage (2,615 m water depth, 35.059°S, 17.401°E) (Hall et al., 2017). The spliced composite record for this

site is 323 m CCSF with a shipboard derived age model based average sedimentation rate of ~5 cm/kyr (Hall et al., 2017).

2.2. Stable Isotope Analyses

Stable isotopes were measured on a single morphotype of the epibenthic foraminifer *Cibicidoides wuellerstorfi* picked from the >150 μm size fraction of sediment at 5 cm intervals. Carbon and oxygen isotopes were measured on a Thermo MAT 253 mass spectrometer equipped with a Kiel IV carbonate preparation device at Scripps Institution of Oceanography. Long-term analytical reproducibility was 0.06‰ for $\delta^{18}O$ and 0.04‰ for $\delta^{13}C$ 1σ, based on ~250 repeated measurements of the NBS-19 carbonate standard. Isotope ratios are reported relative to the Vienna Pee Dee Belemnite standard.

2.3. Neodymium Isotope Analyses

Neodymium isotopes were measured on carbonates from the 63 to 150 μm size fraction of the bulk sediment. Site U1479 has relatively high carbonate (the upper 6.5 m CCSF, equivalent to the last 165 kyr, has an average carbonate content of 64 wt. %), and this sieve fraction primarily consists of small foraminifera and foraminifera fragments. Each Nd isotope measurement was done on approximately 50–70 mg of this foraminifera fraction. Residual clays were removed using established methodology for measurement of Nd isotopes on foraminifera (Palmer & Elderfield, 1985; Roberts et al., 2010), and samples were dissolved in 3M acetic acid. Biogenic carbonates contain organic carbon that serves as templating material for biomineralization that can interfere with column chromatography and effect mass fractionation during inductively coupled plasma (ICP) mass spectrometry. To oxidize this residual organic matter: samples were re-dissolved in 1 mL of 50% aqua regia (made with double distilled HNO_3 and HCl), refluxed at 150°C for a minimum of 4 h and dried down, then re-dissolved again in 1 mL of double distilled concentrated HNO_3, refluxed at 150°C for a minimum of 4 h, dried down, and finally re-dissolved in 500 μL of 1N HNO_3 for column chemistry. Nd was separated from other elements following established methodology: rare earth elements (REEs) were separated using Eichrom TRU resin (100–150 μm mesh) loaded in 250 μL Teflon microvolume columns, and then Nd was separated from other REEs using Eichrom LN resin (50–100 μm mesh) loaded into calibrated 5 mL Teflon columns.

Nd concentrations before and after column chemistry were determined by measurement on a VG PQ ExCell quadrupole ICP-MS. The Nd isotopic composition was measured on a ThermoScientific Neptune-PLUS multicollector (MC) ICP-MS at the Lamont-Doherty Earth Observatory of Columbia University using either H + standard or X + Jet cones and equipped with either an ESI Apex IR or a Cetac Aridus 3 desolvating nebulizer. Instrument stability was determined by monitoring the reproducibility of the JNdi-1 Nd isotope standard (i.e., intermediate error), and it was typically between 0.2 and 0.3 εNd units. Sample $^{143}Nd/^{144}Nd$ values were corrected using an exponential mass fractionation law to $^{146}Nd/^{144}Nd = 0.7219$, using concentration matched, mass-bias corrected bracketing JNdi-1 standards (Tanaka et al., 2000). Sample uncertainties are reported as the 2σ standard deviation of the JNdi-1 standards run during that measurement session, accounting for any long-term drift in the measurement ratio, and they range from 0.13 to 0.41 εNd units. Additional information about analytical quality assurance is provided in the Supporting Information S1.

2.4. Site U1479 Core Chronology and Stratigraphic Correlation of Other Cape Basin Records

The goal of using the new εNd and $\delta^{13}C$ data with previously published records from other depths in the Cape Basin (see Table 1) requires relatively precise stratigraphic correlation (<a few thousand years). To achieve this correlation, we have used the benthic $\delta^{18}O$ data from sediment core MD02-2588, collected from the southwestern flank of the Agulhas Plateau, as a regional benchmark tuning target because of its high resolution and temporal extent (covering the past ~350 kyr) (Ziegler et al., 2013). We graphically tuned the benthic $\delta^{18}O$ records from all the Cape Basin sites to this benchmark in the depth domain. For Site U1479, which is at a very similar water depth to MD02-2588 (2,625 m vs. 2,907 m, respectively), we also assume that it lies on the same isopycnal surface as MD02-2588 (see Figure 1) and should therefore have the same benthic $\delta^{18}O$ composition within analytical error (±0.1‰). Once all cores were aligned, we applied an age model that combines the extensive ^{14}C chronology from site TN057-21 (Barker et al., 2010)

Table 1
Locations of Cores Used in This Study

Core name	Water depth (m)	Latitude (°N)	Longitude (°E)	Reference
ODP 1087	1,372	−31.465	15.311	(Hu et al., 2016; Pierre et al., 2001)
ODP 1088	2,082	−41.136	13.563	(Hodell et al., 2003; Hu et al., 2016)
U1479	2,615	−35.055	17.401	This Study
MD02-2588	2,907	−41.332	25.828	(Ziegler et al., 2013)
TN057-6	3,751	−42.873	8.973	(Hartman, 2015; Hodell et al., 2003)
ODP 1089	4,621	−40.937	9.894	(Charles et al., 2010)
RC11-83	4,718	−41.600	9.800	(Charles et al., 1996; Piotrowski et al., 2005)
TN057-21	4,981	−41.133	7.817	(Barker et al., 2010; Ninnemann & Charles, 2002; Piotrowski et al., 2005)

for the upper ~40 ka of the record, with the EDC-tuned chronology of the deeper section of the MD02-2588 record (Ziegler et al., 2013). The resulting chronology is primarily for convenient external reference—it is the relative stratigraphic correlation among cores that is most important for our purposes here. Stable isotope data for all cores except TN057-21 and RC11-83 covers the interval from 0 to 350 kyr, εNd data for Sites U1479, 1087, and 1088 covers the interval from 0 to 150 kyr, and εNd data from Sites TN057-21 and RC11-83 are combined to make a single composite record from 0 to 100 kyr (Piotrowski et al., 2005). Sedimentation rates range from almost 20 cm/kyr at Site RC11-83, ~15 cm/kyr at Sites TN057-21 and 1089, 5 cm/kyr at Site U1479, 3.4 cm/kyr at Site MD02-2588, 2.3 cm/kyr at Site 1087, and 1 cm/kyr at Site 1088. Sampling resolutions for these cores range from ~300-year at Site MD02-2588 and for the combined RC11-83/TN057-21 record, ~450-year for Site 1089, 1000-year for Site U1479, and ~2000-year for Sites 1087 and 1088.

To examine changes in water mass structure over time, we used these chronologically aligned records to calculate vertical carbon and neodymium isotope gradients. First, all carbon and neodymium isotope records were interpolated at 500-year resolution to a common age vector, then data were smoothed with a butterworth lowpass filter to remove high-frequency variability. Error on this smoothed fit was estimated using a Monte Carlo method, applying 500-year age errors, 0.1‰ $\delta^{13}C$ errors, and 0.2 epsilon unit εNd errors. Error envelope is the 2σ standard deviation of all Monte Carlo iterations at each timestep. Cores were grouped according to depth and smoothed records within each depth group were averaged, where Sites 1087 and 1088 constitute the "intermediate depth" records (1,372–2,082 m), Sites U1479 and MD02-2588 constitute the "mid-depth" records (2,615–2,907 m), and Sites 1089, RC11-83, and TN057-21 constitute the "deep" records (4,618–4,981 m). Finally, vertical gradients were calculated by subtracting these averaged groups from one another.

3. Results

3.1. Site U1479 εNd and Stable Isotopes

Benthic oxygen isotopes at Site U1479 show clear variation over the past 350 kyr (Figure 3a). Average $\delta^{18}O$ values were 2.93‰ for the Holocene, 2.95‰ during Stage 5e, and 4.60‰ at the LGM (Figure 4a). Carbon isotopes also show variations across the major marine isotope stages, but variability across MIS 5 substages is not as pronounced. Average $\delta^{13}C$ values were 0.72‰ during the Holocene and −0.03‰ at the LGM, although the carbon isotope minimum preceded the LGM by around 10 kyr, with a minimum of around −0.16‰ at 30 ka (Figure 4c). Aside from some millennial-scale variability, carbon isotope values were nearly constant during all of MIS 5 at a value of approximately 0.41‰ (±0.2‰ 1σ standard deviation), perhaps increasing slightly between MIS 5e and 5a. Carbon isotope values fell to near-30 ka values during MIS 4 then rose to around 0.25‰ in early MIS 3. At both Terminations 1 and 2, $\delta^{13}C$ increases lead $\delta^{18}O$ decreases by thousands of years (Figure 4).

The co-registered neodymium isotope variations at Site U1479 closely follow carbon isotope variations ($R^2 = 0.54$, $p < 0.001$ based on correlating the raw, non-interpolated data). The εNd record also shows

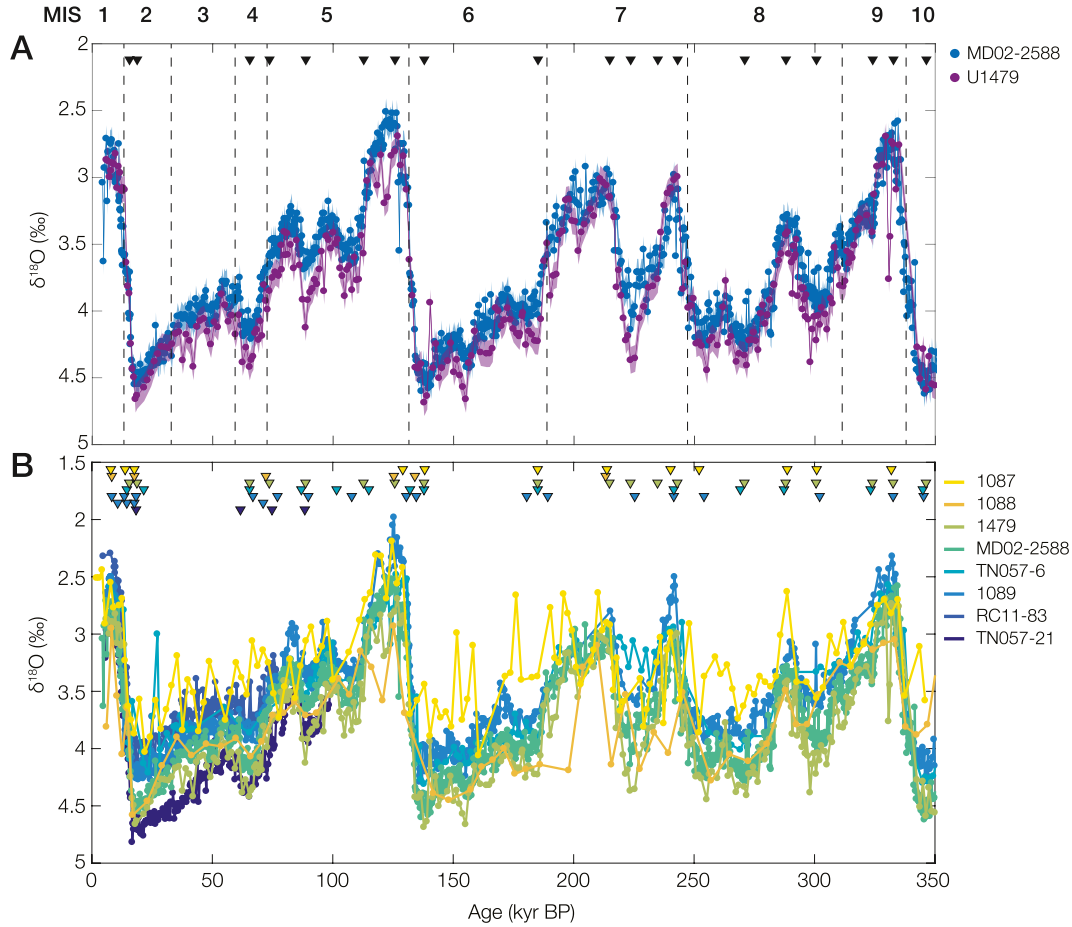

Figure 3. Alignment of Cape Basin records. (a) Site U1479 age model based on alignment with MD02-2588. Shading behind points represents ±0.1‰ agreement criterion for records assumed to share an isopycnal. (b) Stratigraphic alignment of all Cape Basin records to MD02-2588. Inverted triangles mark tie points.

maximum values that precedes the LGM, small variability across the MIS 5 substages, and glacial terminations for MIS 6 and 2 that start earlier and are of longer duration than the $\delta^{18}O$ record (Figure 4b). Average εNd values are −10.56 (±0.18 1σ standard deviation) during the Holocene and −8.68 (±0.20 1σ standard deviation) at the LGM, with maximum of −7.92 at 25 ka. Nd isotope values during MIS 3 are around −10.03 (±0.18 1σ standard deviation) at ~50 ka, around −8.93 (±0.25 1σ standard deviation) at ~64 ka during MIS 4, and around −10.52 (±0.32 1σ standard deviation) at ~77 ka in MIS 5a. There is little εNd variability during MIS 5, with values slightly decreasing across this interval from around −9.8 during MIS 5e to around −10.8 at MIS 5c and 5a. As is seen in the carbon isotope record, the εNd decrease across Termination 2 is much more gradual and starts earlier (around 143 ka) than the oxygen isotope decrease, which begins at ~135 ka. These temporal offsets cannot be attributed to age model uncertainties, since the carbon, oxygen and neodymium isotopes are measured on different size fractions of the same samples.

4. Discussion

4.1. Cape Basin Vertical Neodymium and Carbon Isotope Structure Over the Last 150 kyr

Neodymium isotope records from all Cape Basin cores show similar trends across the past 160 kyr (Figure 5); during warm isotope stages (MIS 1, 3, 5) εNd values are more negative, and during cold isotope stages (MIS 2, 4, 6) εNd values are less negative. Nd isotope values are the most negative during the Holocene (MIS 1), and there is relatively little εNd variation during MIS 5, (for Sites U1479, 1087 and 1088, which go back that far). Site U1479, at 2,615 m water depth, which sits in the core of NADW in the modern Cape Basin

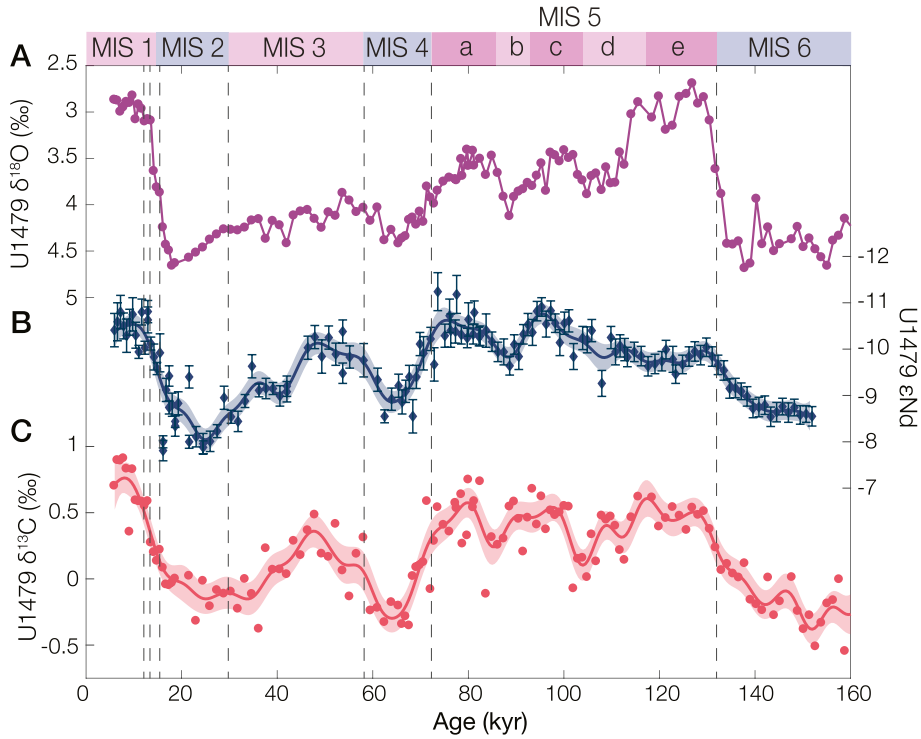

Figure 4. Site U1479 εNd and stable isotopes over the last 150 kyr. Stable oxygen (a) and carbon (c) isotopes measured on *Cibicidoides wullerstorfi* benthic foraminifera. (b) εNd measured on carbonate from the 65 to 150 μm sieve fraction of sediment. εNd and $\delta^{13}C$ data were interpolated at 500-year resolution and smoothed with a lowpass filter (lines and error envelopes, see Section 2.5). Note reversed scale for $\delta^{18}O$ and εNd. Bar at the top marks the marine isotope stages and substages over this time interval (Lisiecki & Raymo, 2005; Railsback et al., 2015).

(Figures 1b and 1c), has the most negative εNd values throughout this entire interval (Figure 5d). This suggests that NADW (or its glacial analogue) did not shoal more than ~500 m over the last glacial cycle—if it had, measured εNd values at Site 1088 should have been more negative than U1479 (as in Figures 2d–2f, Table 1).

Carbon isotope fluctuations are also generally consistent across all depths in the Cape Basin over the last glacial cycle, and they largely follow εNd values (Figure 5e). Carbon isotopes are high in the Holocene, lower during cold stages (MIS 2, 4, 6) and high in past warm stages (MIS 3 and 5). In most cores, $\delta^{13}C$ values are not as high during MIS 3 as during MIS 5, and, while there is some variation during the MIS 5 substages, 5e is not prominently higher in $\delta^{13}C$ than the other MIS 5 substages. As has been discussed previously (e.g., Hodell et al., 2003), $\delta^{13}C$ shifts during cold stages are largest in the deep Cape Basin. At the deepest sites, ODP 1089 and RC11-83 (4,621 and 4,981 m, respectively), values rise from around −1‰ at the LGM to around +0.2‰ during the Holocene. On the other hand, the shallowest cores (ODP 1087 and 1088, at 1,372 and 2,082 m, respectively) show very little change from LGM to Holocene—ODP 1087 essentially has no LGM to Holocene change and ODP 1088 rises from around 0.3 to 0.5‰. Site U1479 and the other intermediate depth site MD02-2588 (2,615 and 2,907 m, respectively), show intermediate changes from around 0‰ at the LGM to 0.6‰ during the Holocene. In contrast to εNd, $\delta^{13}C$ for Site U1479 is not offset toward heavier values compared to shallower sites. This contrasting vertical structure for $\delta^{13}C$ is likely at least partly a product of air-sea gas exchange given that the $\delta^{13}C$ of modern DIC in the 1,000–2,000 m water depth range is significantly (~0.5‰) elevated above expectations from nutrient concentrations alone.

Vertical εNd and $\delta^{13}C$ gradients provide information about the broader water column structure in the Cape Basin, and can help elucidate the mechanisms driving shifts in both tracers across the last glacial cycle (Figure 5). There are no secular trends in the vertical εNd or $\delta^{13}C$ gradients over this time period, but there are short-term variations (~10–20 kyr timescale). Intermediate (1087 and 1088) to mid-depth (U1479) εNd gradients are around 1 εNd unit, and deep to mid-depth εNd gradients are around 2 εNd units. Deep to

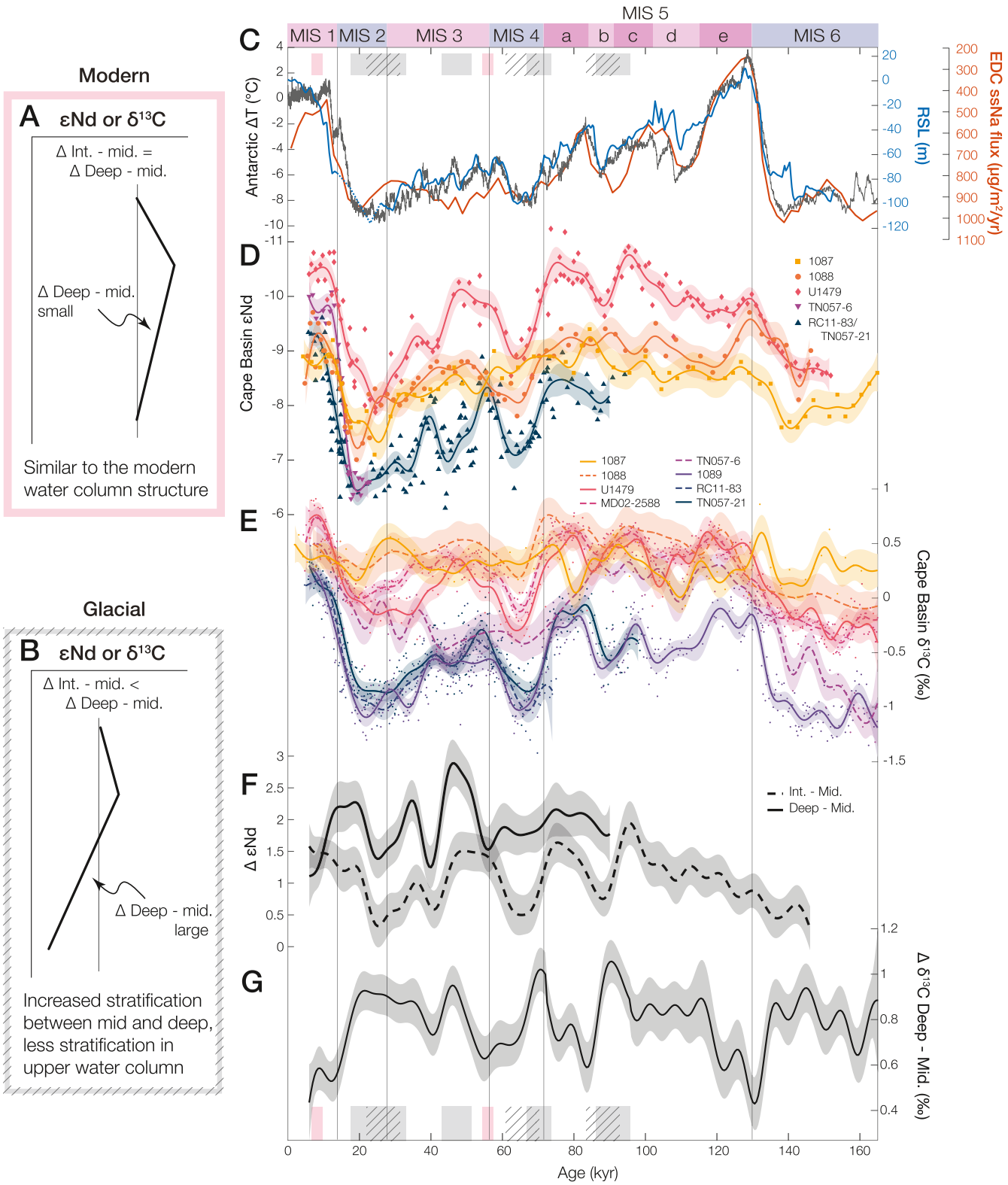
Modern
A εNd or δ13C
Δ Int. - mid. =
Δ Deep - mid.
Δ Deep - mid.
small
Similar to the modern
water column structure
Glacial
B εNd or δ13C
Δ Int. - mid. <
Δ Deep - mid.
Δ Deep - mid.
large
Increased stratification
between mid and deep,
less stratification in
upper water column
MIS 5
MIS 1
MIS 2
MIS 3
MIS 4
a
b
c
d
e
MIS 6
C
Antarctic ΔT (°C)
RSL (m)
EDC ssNa flux (µg/m²/yr)
D
Cape Basin εNd
1087
1088
U1479
TN057-6
RC11-83/
TN057-21
1089
MD02-2588
E
Cape Basin δ13C (‰)
F
Δ εNd
Int. - Mid.
Deep - Mid.
G
Δ δ13C Deep - Mid. (‰)
Age (kyr)

Figure 5.

mid-depth $\delta^{13}C$ gradients vary around 0.8‰, with a maximum value of 1‰ and a minimum of 0.4‰. Intermediate to mid-depth gradients for $\delta^{13}C$ are not plotted because carbon isotope values for Sites 1087 and 1088 are nearly constant over the last glacial cycle (Figure 5e), and, therefore, the gradients are simply a mirror of the U1479 record itself (these gradients are included in Figure S3 in Supporting Information).

The gradients reveal two distinct water column structures (Figures 5a and 5b) that appear at various times across the last glacial cycle. The first is similar to the modern (Figure 5a), where intermediate to mid-depth gradients are approximately equal to deep to mid-depth gradients. This structure is present in the mid-Holocene and at the MIS 4/3 transition, marked in pink below Figures 5f and 5g. The other configuration approaches what has been proposed for the LGM, with smaller intermediate to mid-depth gradients and larger mid to deep gradients (Figure 5b), indicating a reduction in northern-sourced water at depth and a relative increase in the upper water column. Unlike some conceptions of glacial water mass structure, our data indicate that the core of NADW does not shoal when intermediate to mid and mid to deep gradients change. Periods with small intermediate to mid gradients (for εNd) are marked with diagonally hatched bars below Figures 5f and 5g, and those with large mid to deep gradients are marked with gray bars. This structure first appears late in MIS 5 and persists through much of the glacial, especially at the MIS 5/4, and 3/2 transitions, but as noted is broken by the modern-like structure at the MIS 4/3 transition.

4.2. Circulation Changes Over the Last Glacial Cycle

The ocean circulation structure that was originally inferred from carbon isotopes, with NADW shoaled above 2,000 m in the Atlantic (Curry & Oppo, 2005; Ferrari et al., 2014), is quite different from the structure implied by Nd isotope measurements in the Cape Basin, with Nd isotope shifts recorded throughout the water column. This potentially indicates a change in endmember value rather than a dramatic change in the vertical water mass structure (Howe et al., 2016; Pöppelmeier et al., 2020; Zhao et al., 2019). Overall, our new data are consistent with previous Nd isotope data and updated carbon isotope compilations (Oppo et al., 2018), supporting a more modest change in vertical structure.

The $\delta^{13}C$ and εNd data contoured in depth and time (Figure 6) make the water mass dynamics in the Cape Basin more apparent. Pink, gray, and diagonally hatched bars in Figure 6 are the same as in Figure 5, indicating a "modern" (pink) or "glacial" water column structure, with increased mid to deep stratification (gray) and decreased intermediate to mid-depth stratification (hatched). At around 100 ka (when the deep εNd record begins), increases in deep stratification are driven by changes at depth toward increased εNd values and decreased $\delta^{13}C$ values. This time period coincides with the early stages of glacial inception, characterized by decreased temperatures and increased sea ice extent around Antarctica (Figure 5c). About 20 kyr later, approaching the MIS 5/4 transition, the same glacial structure is observed, this time driven by changes throughout the water column (seen especially in Figure 6c). The return to a modern-like water column structure at the MIS 4/3 transition is also driven by changes throughout the water column, coinciding with a modest increase in temperature and sea level (Figure 5c). Through the rest of MIS 3 into MIS 2, εNd and $\delta^{13}C$ shifts start in the deep Cape Basin then progress to shallower depths (Figure 6).

The relative timing of shallow, mid-depth, and abyssal shifts in carbon and neodymium isotopes provide information about the potential mechanisms of change across the last glacial cycle. Abyssal water in the Cape Basin is sourced from a mixture of Weddell Sea Bottom Water and Lower Circumpolar Deep Water (Orsi et al., 1999). Increases in sea ice extent in the latter part of MIS 5 could have contributed to water

Figure 5. Compiled Cape Basin εNd and $\delta^{13}C$ data with schematic water column profiles and global climate data. (a) A schematic "modern" profile, where gradient between intermediate and mid-depth is approximately equal to gradient between mid-depth and deep. (b) A schematic "glacial" profile, with reduced gradient between intermediate and mid-depth and increased gradient between mid-depth and deep. (c) Global climate data including Antarctic temperature difference from the modern (gray) (Parrenin et al., 2013), relative sea level (blue) (Grant et al., 2012), and EDC sea-salt sodium (ssNa), where high values are a proxy for increased sea ice extent (red, inverted axis) (Wolff et al., 2006). (d) Cape Basin εNd data from Sites 1087 and 1088 (Hu et al., 2016), Site U1479 (This Study), TN057-6 (Hartman, 2015), and the combined RC11-83/TN057-21 record (Piotrowski et al., 2005). (e) $\delta^{13}C$ data from cores ODP 1087 and 1088 (Hu et al., 2016), U1479 (This Study), MD02-2588 (Ziegler et al., 2013), TN057-6 (Hodell et al., 2003), ODP 1089 (Charles et al., 2010), RC11-83 (Charles et al., 1996), and TN057-21 (Ninnemann & Charles, 2002). Lines in d and e show data smoothed with a lowpass filter. (f) Vertical εNd gradients between intermediate (1087 and 1088) and mid-depth (U1479) is shown in the dashed line and mid-depth (U1479) to deep (RC11-83/TN057-21) is shown in the solid line. (g) Vertical $\delta^{13}C$ gradient between deep (1089, RC11-83, TN057-21) and mid-depth (MD02-2588 and U1479). See Section 2.5 for information on data smoothing and the calculation of vertical isotope gradients.

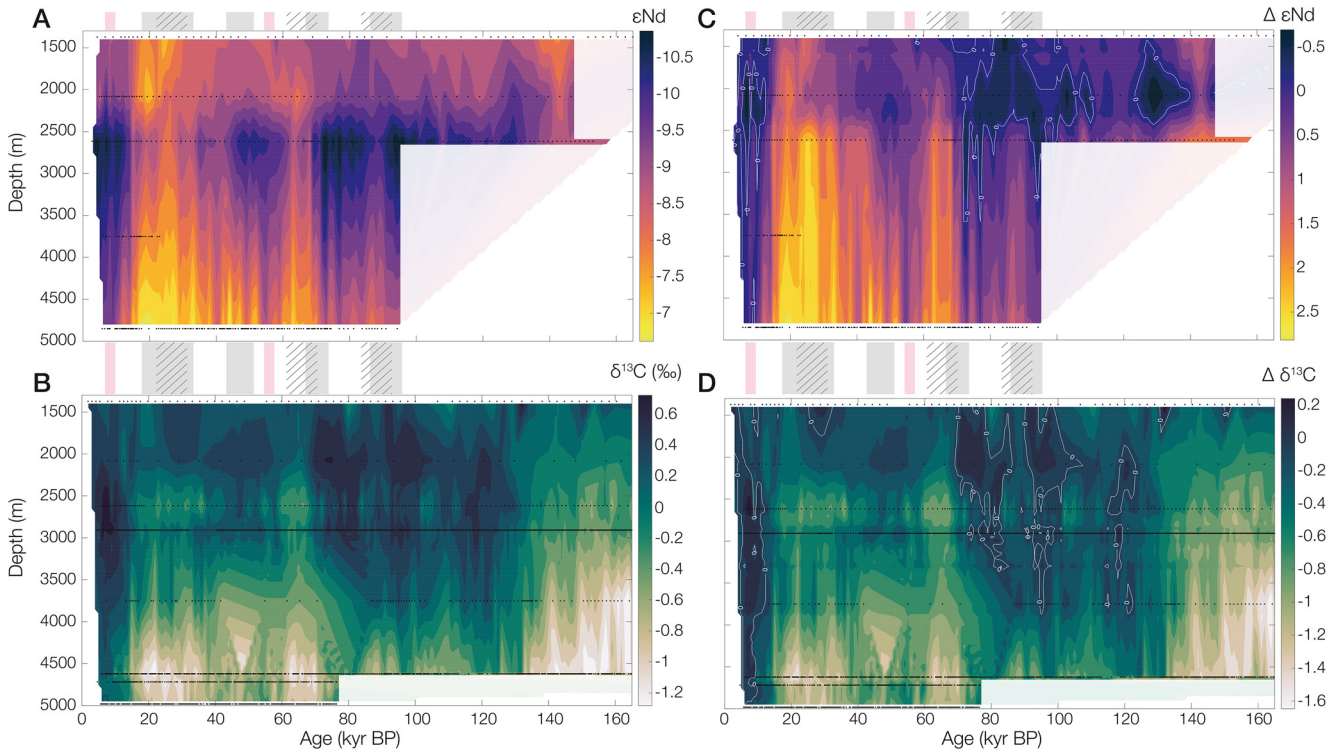

Figure 6. εNd (a), $\delta^{13}C$ (b), ΔεNd (c) and $\Delta\delta^{13}C$ (d) in the Cape Basin over the last 165,000 years. Panels c and d show deviations from late Holocene values (0–6 kyr). Pink, gray, and diagonally hatched bars correspond with Figures 5f and 5g. The pink bar indicates a water column structure similar to the modern, the gray bar indicates an increased gradient between the mid-depth and deep sites, and the hatched bar indicates reduced stratifica- tion between the intermediate and mid-depth sites. In panels c and d, white contours mark the zero line. White boxes cover regions that are not adequately constrained by data.

mass restructuring at this time (Figure 5c) (Wolff et al., 2006). Buoyancy fluxes associated with sea ice production and melt play a primary role in Southern Ocean circulation (Abernathey et al., 2016; Pellichero et al., 2018), and changes in sea ice extent can potentially influence the basin-wide organization of water masses (Ferrari et al., 2014). While we do not see evidence for a dramatic shoaling of NADW at any time over the last glacial cycle, increased mid to deep gradients in εNd and $\delta^{13}C$ could indicate the presence of more southern-sourced deep water, potentially with a larger contribution from the Pacific (as was observed at the LGM by Yu et al., 2020). Increased sea ice can also influence $\delta^{13}C$ values through its influence on the regional extent of air-sea gas exchange (Broecker & Maier-Reimer, 1992; Lynch-Stieglitz & Fairbanks, 1994; Lynch-Stieglitz et al., 1995; Marchitto & Broecker, 2006).

At the MIS 5/4 and 4/3 transitions, as well as in MIS 2, neodymium and carbon isotope shifts occur throughout the water column, indicating that both Northern and Southern Hemispheric processes are contributing to the observed water mass reorganization. Since, mid-depth waters recorded by Site U1479 appear to be influenced by NADW throughout the last glacial cycle, this site should provide information about Northern Hemispheric contributions to observed changes. The deepest sites, which are primarily influenced by southern-sourced water masses, provide information about Southern Hemispheric contributions. Sea ice changes may have played a role in deep Cape Basin εNd and $\delta^{13}C$ shifts during this time, although sea-salt sodium (ssNa, a proxy for sea ice extent) records show less variability at this time compared to late MIS 5 (Figure 5c) (Wolff et al., 2006). For the mid-depth site U1479, εNd variability may have also been influenced by changes in the NADW εNd endmember, which a recent study has suggested to be sensitive to the extent of land ice cover (Zhao et al., 2019) (Figure 5c), especially over the northeastern Canada cratons characterized by the most negative εNd values (Batchelor et al., 2019; Robinson et al., 2021).

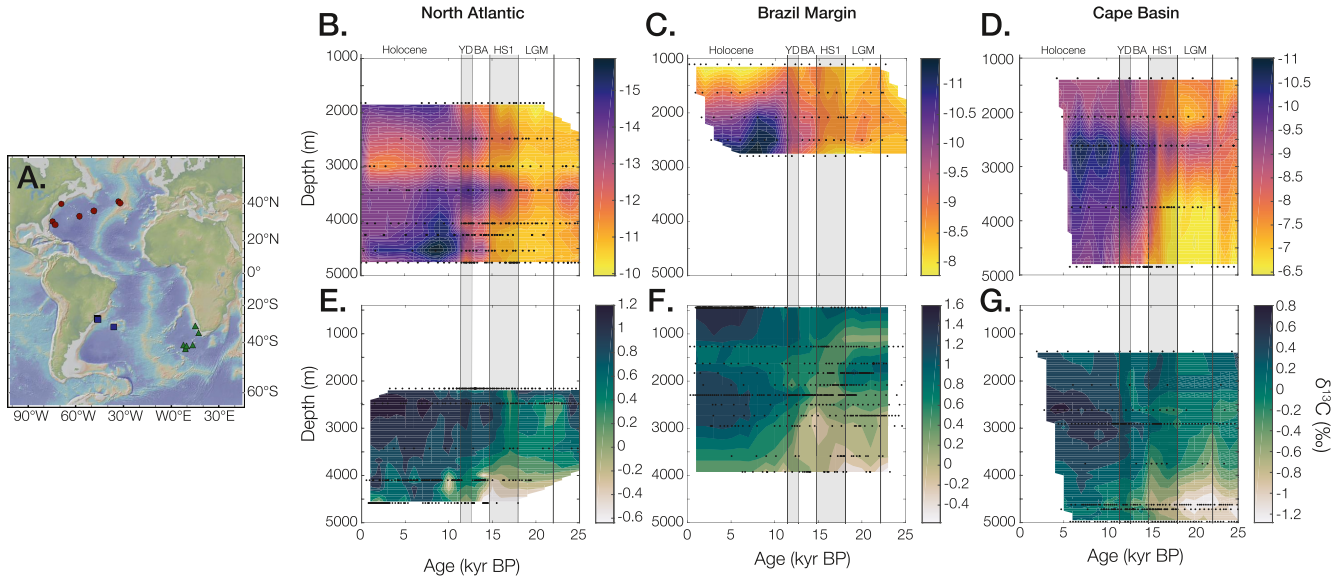

Figure 7. Termination 1 $\delta^{13}C$ and εNd records from across the Atlantic. (a) Map of core locations with red dots marking North Atlantic cores (Howe et al., 2016; Lang et al., 2016; Pöppelmeier et al., 2018, Pöppelmeier, Blaser et al., 2019; Roberts et al., 2010; Zhao et al., 2019), blue squares marking Brazil Margin cores (Lund et al., 2015; Pöppelmeier, Gutjahr et al., 2019) and green triangles marking Cape Basin cores (Charles et al., 1996, 2010; Hartman, 2015; Hodell et al., 2003; Hu et al., 2016; Ninnemann & Charles, 2002; Pierre et al., 2001; Piotrowski et al., 2005; this study). Plots of εNd (b–d) and $\delta^{13}C$ (e–g) from the North Atlantic, Brazil Margin, and Cape Basin, left to right.

4.3. The Effects of North Atlantic and Pacific Endmember Changes on Reconstructed εNd

Changes in the relative mixture of North Atlantic and Pacific-derived water will influence εNd values, but shifts can also arise from changes in endmember composition. Measurements from across the Pacific over the last glacial cycle and beyond indicate relatively constant εNd values (Abouchami et al., 1997; Hu & Piotrowski, 2018), but evidence for changes in the North Atlantic endmember is still equivocal (Foster et al., 2007; Kim et al., 2021; Pöppelmeier et al., 2021; van de Flierdt et al., 2006; Zhao et al., 2019). High-resolution sediment core data from the past ~100 kyr indicate that the NADW endmember changed (Lang et al., 2016; Pöppelmeier et al., 2021; Zhao et al., 2019), while Fe-Mn crust and deep-sea coral data suggest that NADW values were constant. However, limited sampling resolution due to low Fe-Mn crust accumulation rates (Foster et al., 2007) and discontinuous fossil coral sample availability (van de Flierdt et al., 2006) make NADW endmember temporal evolution challenging to explicitly determine. Data from three depth transects spanning the Atlantic over Termination 1 (Figures 7b–7d) indicate that LGM εNd values were higher throughout the water column, with only modest changes in vertical structure (Howe et al., 2016; Lang et al., 2016; Pöppelmeier et al., 2018; Pöppelmeier, Blaser et al., 2019; Pöppelmeier, Gutjahr et al., 2019; Roberts et al., 2010; Zhao et al., 2019). The North Atlantic transect in particular has a similar vertical water column structure at the LGM compared to the modern, with the lowest glacial εNd values around 3,000 m (Zhao et al., 2019), at the same time all εNd values are shifted toward higher values than today, which may indicate a higher εNd endmember value for NADW at the LGM.

We can quantitatively assess the impact of changing endmember εNd values by per-forming a mixing calculation:

$$f_{\mathrm{NADW}} = \frac{R_P \times [Nd]_P - R_{\mathrm{samp}} \times [Nd]_P}{R_{\mathrm{samp}} \times \left([Nd]_N - [Nd]_P\right) - R_N \times [Nd]_N + R_P \times [Nd]_P} \quad (1)$$

where "f_{NADW}" is the fraction of NADW, "R" is the $^{143}Nd/^{144}Nd$, [Nd] is the neodymium concentration, and the subscripts "P" and "N" refer to PDW and NADW, respectively. Although we apply a binary mixing calculation here, we acknowledge that Southern Ocean sourced waters may also play a role in setting εNd values in the Cape Basin. However, given our inability to deconvolve more than two endmembers with a single

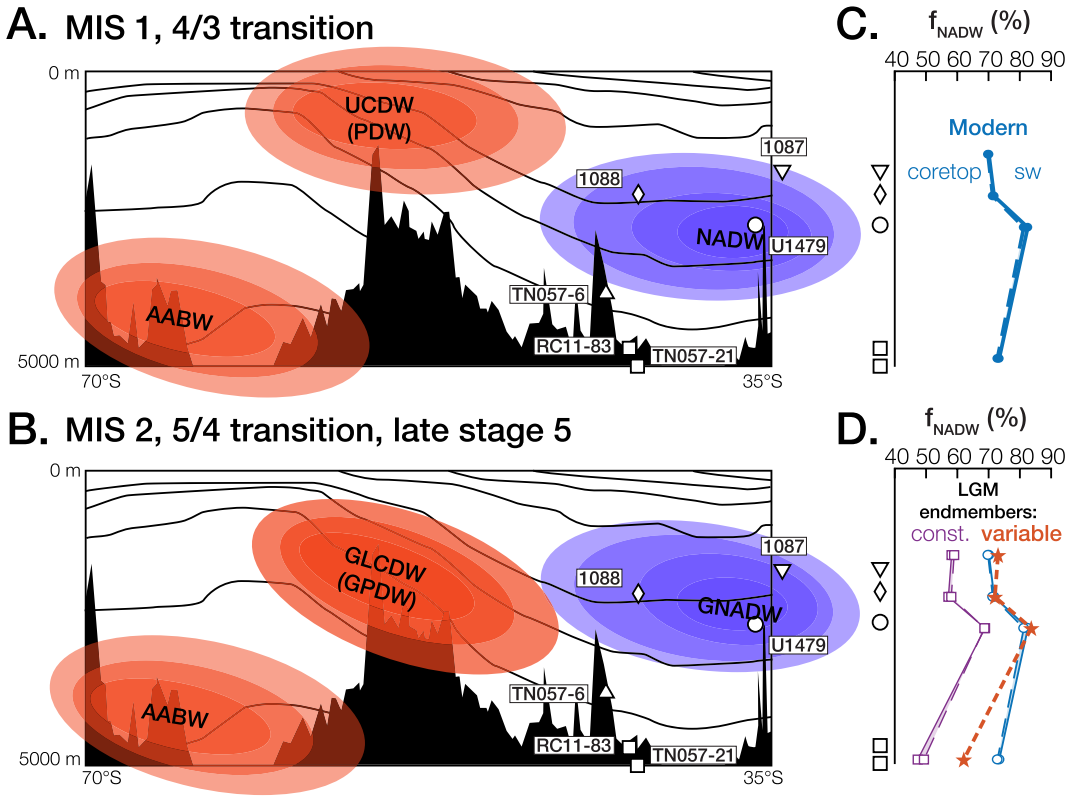

Figure 8. Revised circulation schematic for the Cape Basin over the last glacial cycle. (a) Water mass distribution in the Cape Basin in the Modern and at the MIS 4/3 transition. (b) Water mass distribution in the Cape Basin at the Last Glacial Maximum, the MIS 5/4 transition and in late MIS 5. (c) North Atlantic Deep Water (NADW) fraction at each core site for the Modern ocean using seawater endmembers (solid line) and coretop endmembers from (Hu & Piotrowski, 2018) and (Zhao et al., 2019) (dashed line). (d) NADW fraction (vs. PDW) at each core site at the Last Glacial Maximum using constant endmembers (purple squares) or variable endmembers from (Hu & Piotrowski, 2018) and (Zhao et al., 2019) (red stars). Modern f_{NADW} profile also included for comparison (blue). Error bars on f_{NADW} are smaller than the points.

isotope system, and the many additional assumptions that would be required to incorporate $\delta^{13}C$ along with εNd into the mixing calculation, examining mixing between NADW and PDW at the LGM is an appropriate and informative simplification.

In the modern ocean, the NADW fraction can be calculated either by using seawater εNd values (Figure 8c solid line) or sediment coretop values (Figure 8c dashed line). North Atlantic coretops are between −13 and −14, with values of −13.4 at 3,426 m water depth (Lang et al., 2016), −13.2 at 2,475 m water depth (Howe et al., 2016), and −14 at 1,820 m water depth (Zhao et al., 2019). They closely match seawater values from similar depths, which also range from −13 to −14 (Lambelet et al., 2016). We use a North Atlantic coretop value of −14 from KNR198-GGC35/CDH36/MC37 at 1,820 m water depth (Zhao et al., 2019). This site is in the upper part of modern NADW, but would remain in NADW even if this water mass shoaled at the LGM. Using values from deeper sites would not change our results. In the Pacific, a core-top εNd value of −3 is estimated from an average of equatorial Pacific Sites ODP 846 and V28-239 (Hu & Piotrowski, 2018). For modern PDW, there is no consensus εNd value—North Pacific seawater data cluster around −3 to −4, although measurements range from −6 to −0.7 (Amakawa et al., 2004, 2009; Behrens et al., 2018; Fröllje et al., 2016; Haley et al., 2014; Pahnke et al., 2012; Piepgras & Jacobsen, 1988; Shimizu et al., 1994; Vance et al., 2004; Wu, 2019; Zimmermann et al., 2009). Modern [Nd] are 17.5 pmol/kg for the NADW endmember and 35 pmol/kg for the PDW endmember (e.g., Howe et al., 2016).

If we use the sediment core εNd values of −11 for NADW at the LGM (Howe et al., 2016; Lang et al., 2016; Zhao et al., 2019) and −3 for PDW at the LGM (Hu & Piotrowski, 2018) and their respective coretop εNd

values for the modern (−14 and −3, respectively), with no change in Nd concentration for either endmember (since there is currently no proxy for reconstructing [Nd] in the past), we find that the NADW fraction increases slightly at shallow Site 1087 (although within error), is approximately the same for Sites 1088 and U1479, and decreases at the combined deepest site when comparing the LGM to the modern (Figure 8d, red stars). The largest signal is a decrease in f_{NADW} at the deepest site (−11%). There is a very small increase in f_{NADW} is at Site 1087 (+3%), but Site U1479 still is the f_{NADW} maximum (f_{NADW} = 84%). If the endmembers are assumed constant at their modern values, then the f_{NADW} decreases throughout the water column in the Cape Basin, still with the maximum f_{NADW} at Site U1479 (Figure 8d, purple squares).

Regardless of whether or not the North Atlantic εNd endmember changed at the LGM, we do not find evidence for a significant shoaling of the core of NADW (the εNd value of Site U1479 is always more negative than shallower Sites 1087 and 1088). There are changes in the Cape Basin vertical structure, however, with slightly more NADW in the upper water column and significantly less in the deep (Figures 6 and 8). Using the B/Ca proxy for carbonate ion, Yu et al. (2020) also found evidence for a greater fraction of Pacific-sourced water in the deep Cape Basin. While they argue that this results from a shoaling of NADW, which our data do not support, we similarly do find evidence for a larger fraction of PDW relative to NADW at deep Sites RC11-83/TN057-21.

Greater separation between the circulation cells could be one way to reconcile a larger fraction of Pacific-derived water in the abyssal Cape Basin in the absence of significant shoaling of NADW. This is broadly consistent with the results of (Sun et al., 2018), who show only a ∼250 m shoaling of the boundary between the upper and lower cells, despite increases in AABW density and a greater separation between the circulation cells. Glacial PDW ("GPDW" in Figure 8b) seems to exert a greater influence on the abyssal sites, which today are bathed in a combination of LCDW and AABW, rather than the intermediate depth sites, as in the modern ocean.

Finally, the relative strength of advective transport versus diffusive transport may be important for explaining how the core of NADW remained close to its modern depth at the LGM. Isopycnal diffusivity is very important for mixing tracer signals along isopycnal surfaces, and it is strongly affected by eddy activity (which in turn is affected by wind strength). Where advection dominates, that is, at or near the core of NADW, changes in isopycnal diffusivity—which might be expected as a result of changes in westerly wind strength (Abernathey & Ferreira, 2015; Jones & Abernathey, 2019, 2021)—would have a negligible impact on reconstructed signals. Away from the advective maximum, that is, at Sites 1087, 1088, and the combined RC11-83/TN057-21 site, glacial-interglacial changes in isopycnal diffusivity, driven by changes in wind strength, could have a much larger impact, increasing their NADW fractions (Figure 8d).

5. Conclusions

We have presented a high-resolution neodymium and stable isotope record over the last glacial cycle from IODP Site U1479 in the Cape Basin. At 2,615 m water depth on the South African continental margin, Site U1479 sits at the modern core of North Atlantic Deep Water, and is therefore ideally situated to monitor this water mass over the last glacial cycle. Nd isotopes measured at Site U1479 show strong fluctuations across the last glacial cycle, with less negative εNd values during the cold marine isotope stages (MIS 2,4,6) and more negative εNd values during warm marine isotope stages (MIS 1,3,5). Nd isotopes show very similar patterns to co-registered $\delta^{13}C$ measurements from the core, with light carbon isotopes associated with less negative εNd values.

The large number of existing neodymium and carbon isotope records from the Cape Basin allows us to examine water column structural changes over the last glacial cycle by calculating vertical isotope gradients. Site U1479 has most negative εNd values and the maximum NADW influence over the whole last glacial cycle, precluding a shoaling of the NADW core depth by more than ∼500 m (the difference in depth between U1479 and the next shallower site 1088). Additionally, we find that the glacial water column was characterized by increased stratification between the mid-depth and deep and decreased stratification between the intermediate and mid-depths. This glacial circulation structure first emerged in late MIS 5. At the MIS 4/3 transition, the Cape Basin briefly returned to a modern-like circulation structure, but shifts in the

deep ocean increased deep stratification during MIS 3, and upper ocean circulation changes in late MIS 3 and MIS 2 contributed to a return to the full glacial circulation geometry at this time.

A quantitative Nd-based water mass mixing analysis for the Cape Basin confirms our interpretation based on vertical isotope gradients, and indicates relatively modest changes in vertical circulation structure at the LGM. Site U1479 at 2,615 m remained the f_{NADW} maximum during the LGM (as it is today), there were increases in the f_{NADW} at intermediate depth Sites 1087 and 1088, and a slight f_{NADW} decrease at the abyssal site RC11-83/TN057-21. This pattern could be influenced by wind-driven changes in isopycnal mixing, which increased NADW fractions for the intermediate depth sites, and sea-ice driven increases in the separation between the upper and lower circulation cells, even without NADW shoaling appreciably. This increased stratification and separation between the circulation cells that we observe in the deep Cape Basin could have contributed to increased carbon storage in the deep ocean during the last glacial cycle, despite only modest changes in inferred NADW core depth.

Data Availability Statement

All data presented here are included in supplementary tables and are available in the NOAA/WDS Paleo Archive (https://www.ncei.noaa.gov/access/paleo-search/study/34432). Data from other Cape Basin cores used in this study can be found in Barker et al. (2010), Charles et al. (1996, 2010), Hartman (2015), Hodell et al. (2003), Hu et al. (2016), Pierre et al. (2001), Piotrowski et al. (2005), Ninnemann and Charles (2002), and Ziegler et al. (2013). Other data used in Figure 1 come from GLODAPv2 (Olsen et al., 2016) and the GEOTRACES Intermediate Data Product (Schlitzer et al., 2018). In Figure 7 other data from the North Atlantic can be found in Howe et al. (2016), Lang et al. (2016), Pöppelmeier et al. (2018, 2019a), Roberts et al. (2010), and Zhao et al. (2019) and from the Brazil Margin can be found in Lund et al. (2015) and Pöppelmeier, Gutjahr et al. (2019).

Acknowledgments
This work was supported by NSF grant OCE-1831415 (S. K. V. Hines, S. L. Goldstein., S. R. Hemming.). The authors thank C. Spencer Jones, Frank Pavia, Julia Gottschalk, Allison Franzese, Chiza Mwinde, and Stephen Barker for helpful discussions, and the Expedition 361 Scientific Party and JOIDES Resolution technical staff and crew for all the work done in the collection of the sediments used for this study.

References

Abernathey, R., & Ferreira, D. (2015). Southern Ocean isopycnal mixing and ventilation changes driven by winds. *Geophysical Research Letters*, *42*(2310), 10357–10365. https://doi.org/10.1002/2015gl066238

Abernathey, R. P., Cerovecki, I., Holland, P. R., Newsom, E., Mazloff, M., & Talley, L. D. (2016). Water-mass transformation by sea ice in the upper branch of the Southern Ocean overturning. *Nature Geoscience*, *9*(8), 596–601. https://doi.org/10.1038/ngeo2749

Abouchami, W., Goldstein, S. L., Galer, S. J. G., Eisenhauer, A., & Mangini, A. (1997). Secular changes of lead and neodymium in central Pacific seawater recorded by a Fe-Mn crust. *Geochimica et Cosmochimca Acta*, *61*, 3957–3974. https://doi.org/10.1016/s0016-7037(97)00218-4

Adkins, J. F. (2013). The role of deep ocean circulation in setting glacial climates. *Paleoceanography*, *28*(3), 539–561. https://doi.org/10.1002/palo.20046

Amakawa, H., Nozaki, Y., Alibo, D. S., Zhang, J., Fukugawa, K., & Nagai, H. (2004). Neodymium isotopic variations in Northwest Pacific waters. *Geochimica et Cosmochimica Acta*, *68*(4), 715–727. https://doi.org/10.1016/s0016-7037(03)00501-5

Amakawa, H., Sasaki, K., & Ebihara, M. (2009). Nd isotopic composition in the central North Pacific. *Geochimica et Cosmochimica Acta*, *73*(16), 4705–4719. https://doi.org/10.1016/j.gca.2009.05.058

Arhan, M., Mercier, H., & Park, Y.-H. (2003). On the deep water circulation of the eastern South Atlantic Ocean. *Deep-Sea Research Part I*, *50*(7), 889–916. https://doi.org/10.1016/s0967-0637(03)00072-4

Barker, S., Knorr, G., Vautravers, M. J., Diz, P., & Skinner, L. C. (2010). Extreme deepening of the Atlantic overturning circulation during deglaciation. *Nature Geoscience*, *3*(8), 567–571. https://doi.org/10.1038/ngeo921

Batchelor, C. L., Margold, M., Krapp, M., Murton, D. K., Dalton, A. S., Gibbard, P. L., et al. (2019). The configuration of Northern Hemisphere ice sheets through the Quaternary. *Nature Communications*, *1*. https://doi.org/10.1038/s41467-019-11601-2

Behrens, M. K., Pahnke, K., Schnetger, B., & Brumsack, H.-J. (2018). Sources and processes affecting the distribution of dissolved Nd isotopes and concentrations in the West Pacific. *Geochimica et Cosmochimica Acta*, *222*, 508–534. https://doi.org/10.1016/j.gca.2017.11.008

Bower, A., Lozier, S., Biastoch, A., Drouin, K., Foukal, N., Furey, H., et al. (2019). Lagrangian views of the pathways of the Atlantic meridional overturning circulation. *Journal of Geophysical Research: Oceans*, *99*(8), 5313–5335. https://doi.org/10.1029/2019jc015014

Broecker, W. S., & Maier-Reimer, E. (1992). The influence of air and sea exchange on the carbon isotope distribution in the sea. *Global Biogeochemical Cycles*, *6*, 315–320. https://doi.org/10.1029/92gb01672

Charles, C. D., Lynch-Stieglitz, J., Ninneman, U. S., & Fairbanks, R. G. (1996). Climate connections between the hemispheres revealed by deep sea sediment core/ice core correlations. *Earth and Planetary Science Letters*, *142*, 19–27. https://doi.org/10.1016/0012-821x(96)00083-0

Charles, C. D., Pahnke, K., Zahn, R., Mortyn, P. G., Ninnemann, U., & Hodell, D. A. (2010). Millennial scale evolution of the Southern Ocean chemical divide. *Quaternary Science Reviews*, *29*(3–4), 399–409. https://doi.org/10.1016/j.quascirev.2009.09.021

Curry, W. B., Duplessy, J.-C., Labeyrie, L. D., & Shackleton, N. J. (1988). Changes in the distribution of $\delta^{13}C$ of deep water ΣCO_2 between the Last Glaciation and the Holocene. *Paleoceanography*, *3*(3), 317. https://doi.org/10.1029/pa003i003p00317

Curry, W. B., & Oppo, D. W. (2005). Glacial water mass geometry and the distribution of $\delta^{13}C$ of ΣCO_2 in the western Atlantic Ocean. *Paleoceanography*, *20*(1), PA1017. https://doi.org/10.1029/2004PA001021

Eide, M., Olsen, A., Ninnemann, U. S., & Johannessen, T. (2017). A global ocean climatology of preindustrial and modern ocean $\delta^{13}C$. *Global Biogeochemical Cycles*, *31*(3), 515–534. https://doi.org/10.1002/2016gb005473

Ferrari, R., Jansen, M. F., Adkins, J. F., Burke, A., Stewart, A. L., & Thompson, A. F. (2014). Antarctic sea ice control on ocean circulation in present and glacial climates. *Proceedings of the National Academy of Sciences*, *111*(24), 8753–8758. https://doi.org/10.1073/pnas.1323922111

Foster, G. L., Vance, D., & Prytulak, J. (2007). No change in the neodymium isotope composition of deep water exported from the North Atlantic on glacial-interglacial time scales. *Geology*, *35*, 37–40. https://doi.org/10.1130/g23204a.1

Frank, M. (2002). Radiogenic Isotopes: Tracers of past ocean circulation and erosional input. *Reviews of Geophysics*, *40*(1), 11–138. https://doi.org/10.1029/2000rg000094

Fröllje, H., Pahnke, K., Schnetger, B., Brumsack, H.-J., Dulai, H., & Fitzsimmons, J. N. (2016). Hawaiian imprint on dissolved Nd and Ra isotopes and rare earth elements in the central North Pacific: Local survey and seasonal variability. *Geochimica et Cosmochimica Acta*, *189*, 110–131. https://doi.org/10.1016/j.gca.2016.06.001

Garcia-Solsona, E., Jeandel, C., Labatut, M., Lacan, F., Vance, D., Chavagnac, V., & Pradoux, C. (2014). Rare earth elements and Nd isotopes tracing water mass mixing and particle-seawater interactions in the SE Atlantic. *Geochimica et Cosmochimica Acta*, *125*(C), 351–372. https://doi.org/10.1016/j.gca.2013.10.009

Garzoli, S. L., Dong, S., Fine, R., Meinen, C. S., Perez, R. C., Schmid, C., et al. (2015). The fate of the Deep Western Boundary Current in the South Atlantic. *Deep Sea Research Part I: Oceanographic Research Papers*, *103*, 125–136. https://doi.org/10.1016/j.dsr.2015.05.008

Gebbie, G. (2014). How much did Glacial North Atlantic Water shoal? *Paleoceanography*, *29*(3), 190–209. https://doi.org/10.1002/2013pa002557

Goldstein, S., & Hemming, S. R. (2003). Long-lived isotopic tracers in oceanography, paleoceanography, and ice-sheet dynamics. In *Treatise on Geochemistry*, Elsevier, 453–489. https://doi.org/10.1016/b0-08-043751-6/06179-x

Goldstein, S., & O'Nions, R. K. (1981). Nd and Sr isotopic relationships in pelagic clays and ferromanganese deposits. *Nature*, *292*(5821), 324–327. https://doi.org/10.1038/292324a0

Goldstein, S. L., O'Nions, R. K., & Hamilton, P. J. (1984). A Sm-Nd isotopic study of atomospheric dusts and particulates from major river system. *Earth and Planetary Science Letters*, *70*, 221–236. https://doi.org/10.1016/0012-821x(84)90007-4

Grant, K. M., Rohling, E. J., Bar-Matthews, M., Ayalon, A., Medina-Elizalde, M., Ramsey, C. B., et al. (2012). Rapid coupling between ice volume and polar temperature over the past 150,000 years. *Nature*, *491*(7426), 744–747. https://doi.org/10.1038/nature11593

Gu, S., Liu, Z., Oppo, D. W., Lynch-Stieglitz, J., Jahn, A., Zhang, J., & Wu, L. (2020). Assessing the potential capability of reconstructing glacial Atlantic water masses and AMOC using multiple proxies in CESM. *Earth and Planetary Science Letters*, *541*, 116294. https://doi.org/10.1016/j.epsl.2020.116294

Haley, B. A., Frank, M., Hathorne, E., & Pisias, N. (2014). Biogeochemical implications from dissolved rare earth element and Nd isotope distributions in the Gulf of Alaska. *Geochimica et Cosmochimica Acta*, *126*(C), 455–474. https://doi.org/10.1016/j.gca.2013.11.012

Hall, I. R., Hemming, S. R., LeVay, L. J., Barker, S., Berke, M. A., Brentegani, L., et al. (2017). Expedition 361 summary, (Vol. *361*, pp.1–33). *Proceedings of the International Ocean Discovery Program*. https://doi.org/10.14379/iodp.proc.361.101.2017

Hartman, A. E. (2015). *The neodymium composition of Atlantic Ocean watermasses: Implications for the past and present*.

Hodell, D. A., Venz, K. A., Charles, C. D., & Ninnemann, U. S. (2003). Pleistocene vertical carbon isotope and carbonate gradients in the South Atlantic sector of the Southern Ocean. *Geochemistry, Geophysics, Geosystems*, *4*(1), 1–9. https://doi.org/10.1029/2002gc000367

Howe, J. N. W., Piotrowski, A. M., Noble, T. L., Mulitza, S., Chiessi, C. M., & Bayon, G. (2016). North Atlantic Deep Water Production during the Last Glacial Maximum. *Nature Communications*, *7*, 1–8. https://doi.org/10.1038/ncomms11765

Hu, R., Noble, T. L., Piotrowski, A. M., McCave, I. N., Bostock, H. C., & Neil, H. L. (2016). Neodymium isotopic evidence for linked changes in Southeast Atlantic and Southwest Pacific circulation over the last 200 kyr. *Earth and Planetary Science Letters*, *455*(C), 106–114. https://doi.org/10.1016/j.epsl.2016.09.027

Hu, R., & Piotrowski, A. M. (2018). Neodymium isotope evidence for glacial-interglacial variability of deepwater transit time in the Pacific Ocean. *Nature Communications*, *9*(1), 4709. https://doi.org/10.1038/s41467-018-07079-z

Jacobsen, S. B., & Wasserburg, G. J. (1980). Sm-Nd isotopic evolution of chondrites. *Earth and Planetary Science Letters*, *50*, 139–155. https://doi.org/10.1016/0012-821x(80)90125-9

Jeandel, C., Arsouze, T., Lacan, F., Téchiné, P., & Dutay, J. C. (2007). Isotopic Nd compositions and concentrations of the lithogenic inputs into the ocean: A compilation, with an emphasis on the margins. *Chemical Geology*, *239*(1–2), 156–164. https://doi.org/10.1016/j.chemgeo.2006.11.013

Jones, C. S., & Abernathey, R. P. (2019). Isopycnal mixing controls deep ocean ventilation. *Geophysical Research Letters*, *46*(22), 13144–13151. https://doi.org/10.1029/2019gl085208

Jones, C. S., & Abernathey, R. P. (2021). Modeling water-mass distributions in the modern and LGM ocean: Circulation change, isopycnal and diapycnal mixing. *Journal of Physical Oceanography*, *51*(5), 1–48. https://doi.org/10.1175/jpo-d-20-0204.1

Kersalé, M., Perez, R. C., Speich, S., Meinen, C. S., Lamont, T., Hénaff, M. L., et al. (2019). Shallow and Deep Eastern Boundary Currents in the South Atlantic at 34.5°S: Mean structure and variability. *Journal of Geophysical Research-Oceans*, *124*(3), 1634–1659. https://doi.org/10.1029/2018jc014554

Kim, J., Goldstein, S. L., Pena, L. D., Jaume-Seguí, M., Knudson, K. P., Yehudai, M., & Bolge, L. (2021). North Atlantic Deep Water during Pleistocene interglacials and glacials. *Quaternary Science Reviews*, *269*, 107146. https://doi.org/10.1016/j.quascirev.2021.107146

Lambelet, M., van de Flierdt, T., Crocket, K., Rehkämper, M., Kreissig, K., Coles, B., et al. (2016). Neodymium isotopic composition and concentration in the western North Atlantic Ocean: Results from the GEOTRACES GA02 section. *Geochimica et Cosmochimica Acta*, *177*(C), 1–29. https://doi.org/10.1016/j.gca.2015.12.019

Lang, D. C., Bailey, I., Wilson, P. A., Chalk, T. B., Foster, G. L., & Gutjahr, M. (2016). Incursions of southern-sourced water into the deep North Atlantic during late Pliocene glacial intensification. *Nature Geoscience*, *9*(5), 375–379. https://doi.org/10.1038/ngeo2688

Lisiecki, L. E., & Raymo, M. E. (2005). A Pliocene-Pleistocene stack of 57 globally distributed benthic $\delta^{18}O$ records. *Paleoceanography*, *20*(1), PA1003. https://doi.org/10.1029/2004pa001071

Lund, D. C., Adkins, J. F., & Ferrari, R. (2011). Abyssal Atlantic circulation during the Last Glacial Maximum: Constraining the ratio between transport and vertical mixing. *Paleoceanography*, *26*(1), PA1213. https://doi.org/10.1029/2010pa001938

Lund, D. C., Tessin, A. C., Hoffman, J. L., & Schmittner, A. (2015). Southwest Atlantic water mass evolution during the last deglaciation. *Paleoceanography*, *30*(5), 477–494. https://doi.org/10.1002/2014pa002657

Lynch-Stieglitz, J., & Fairbanks, R. G. (1994). A conservative tracer for glacial ocean circulation from carbon isotope and palaeo-nutrient measurements in benthic foraminifera. *Nature*, *369*(6478), 308–310. https://doi.org/10.1038/369308a0

Lynch-Stieglitz, J., Stocker, T. F., Broecker, W., & Fairbanks, R. (1995). The influence of air-sea exchange on the isotopic composition of oceanic carbon: Observations and modeling. *Global Biogeochemical Cycles*, *9*, 653–665. https://doi.org/10.1029/95gb02574

Marchitto, T. M., & Broecker, W. S. (2006). Deep water mass geometry in the glacial Atlantic Ocean: A review of constraints from the paleonutrient proxy Cd/Ca. *Geochemistry, Geophysics, Geosystems*, *7*(12), Q12003. https://doi.org/10.1029/2006gc001323

Ninnemann, U. S., & Charles, C. D. (2002). Changes in the mode of Southern Ocean circulation over the last glacial cycle revealed by foraminiferal stable isotopic variability. *Earth and Planetary Science Letters*, *201*(2). https://doi.org/10.1016/s0012-821x(02)00708-2

Olsen, A., Key, R. M., Heuven, S. van., Lauvset, S. K., Velo, A., Lin, X., et al. (2016). The Global Ocean Data Analysis Project version 2 (GLODAPv2)-An internally consistent data product for the world ocean. *Earth System Science Data*, *8*(2), 297–323. https://doi.org/10.5194/essd-8-297-2016

Oppo, D. W., & Fairbanks, R. G. (1987). Variability in the deep and intermediate water circulation of the Atlantic Ocean during the past 25,000 years: Northern Hemisphere modulation of the Southern Ocean. *Earth and Planetary Science Letters*, *86*, 1–15. https://doi.org/10.1016/0012-821x(87)90183-x

Oppo, D. W., Gebbie, G., Huang, K.-F., Curry, W. B., Marchitto, T. M., & Pietro, K. R. (2018). Data constraints on Glacial Atlantic Water mass geometry and properties. *Paleoceanography and Paleoclimatology*, *298*(5599), 1769–22. https://doi.org/10.1029/2018pa003408

Orsi, A. H., Johnson, G. C., & Bullister, J. L. (1999). Circulation, mixing, and production of Antarctic Bottom Water. *Progress in Oceanography*, *43*(1), 55–109. https://doi.org/10.1016/s0079-6611(99)00004-x

Pahnke, K., van de Flierdt, T., Jones, K. M., Lambelet, M., Hemming, S. R., & Goldstein, S. L. (2012). GEOTRACES intercalibration of neodymium isotopes and rare earth element concentrations in seawater and suspended particles. Part 2: Systematic tests and baseline profiles. *Limnology and Oceanography: Methods*, *10*(4), 252–269. https://doi.org/10.4319/lom.2012.10.252

Palmer, M. R., & Elderfield, H. (1985). Variations in the Nd isotopic composition of foraminifera from Atlantic Ocean sediments. *Earth and Planetary Science Letters*, *73*(2–4), 299–305. https://doi.org/10.1016/0012-821x(85)90078-0

Parrenin, F., Masson-Delmotte, V., Kohler, P., Raynaud, D., Paillard, D., Schwander, J., et al. (2013). Synchronous change of atmospheric CO_2 and Antarctic temperature during the last deglacial warming. *Science*, *339*(6123), 1060–1063. https://doi.org/10.1126/science.1226368

Pellichero, V., Sallée, J.-B., Chapman, C. C., & Downes, S. M. (2018). The southern ocean meridional overturning in the sea-ice sector is driven by freshwater fluxes. *Nature Communications*, *9*(1), 1–9. https://doi.org/10.1038/s41467-018-04101-2

Piepgras, D., & Jacobsen, S. B. (1988). The isotopic composition of neodymium in the North Pacific. *Geochimica et Cosmochimica Acta*, *52*(6), 1373–1381. https://doi.org/10.1016/0016-7037(88)90208-6

Piepgras, D., Wasserburg, G., & Dasch, E. J. (1979). The isotopic composition of Nd in different ocean masses. *Earth and Planetary Science Letters*, *45*, 223–236. https://doi.org/10.1016/0012-821x(79)90125-0

Pierre, C., Saliege, J. F., Urrutiaguer, M. J., & Giraudeau, J. (2001). Stable isotope record of the last 500 k.y. at Site 1087 (Southern Cape Basin). *Proceedings of the International Ocean Discovery Program*, *175*, 1–22. https://doi.org/10.2973/odp.proc.sr.175.230.2001

Piotrowski, A. M., Goldstein, S. L., Hemming, S. R., & Fairbanks, R. G. (2005). Temporal relationships of carbon cycling and ocean circulation at glacial boundaries. *Science*, *307*, 1933–1938. https://doi.org/10.1126/science.110723910.1126/science.1104883

Pöppelmeier, F., Blaser, P., Gutjahr, M., Jaccard, S. L., Frank, M., Max, L., & Lippold, J. (2020). Northern-sourced water dominated the Atlantic Ocean during the Last Glacial Maximum. *Geology*, *48*(8), 1–4. https://doi.org/10.1130/g47628.1

Pöppelmeier, F., Blaser, P., Gutjahr, M., Jaccard, S. L., Frank, M., Max, L., & Lippold, J. (2019). Influence of ocean circulation and benthic exchange on Deep Northwest Atlantic Nd Isotope records during the past 30,000 years. *Geochemistry, Geophysics, Geosystems*, *25*, 3246–13. https://doi.org/10.1029/2019gc008271

Pöppelmeier, F., Gutjahr, M., Blaser, P., Keigwin, L. D., & Lippold, J. (2018). Origin of Abyssal NW Atlantic water masses since the last glacial maximum. *Paleoceanography and Paleoclimatology*, *33*, 530–543. https://doi.org/10.1029/2017pa003290

Pöppelmeier, F., Gutjahr, M., Blaser, P., Oppo, D. W., Jaccard, S. L., Regelous, M., et al. (2019). Water mass gradients of the mid-depth Southwest Atlantic during the past 25,000 years. *Earth and Planetary Science Letters*. *531*(1). https://doi.org/10.1016/j.epsl.2019.115963

Pöppelmeier, F., Gutjar, M., Blaser, P., Schulz, H., Süfke, F., & Lippold, J. (2021). Stable Atlantic deep water mass sourcing on glacial-interglacial timescales. *Geophysical Research Letters*. *48*(15), e2021GL092722. https://doi.org/10.1029/2021GL092722

Rahlf, P., Hathorne, E., Laukert, G., Gutjahr, M., Weldeab, S., & Frank, M. (2019). Tracing water mass mixing and continental inputs in the southeastern Atlantic Ocean with dissolved neodymium isotopes. *Earth and Planetary Science Letters*, *530*, 115944. https://doi.org/10.1016/j.epsl.2019.115944

Railsback, L. B., Gibbard, P. L., Head, M. J., Voarintsoa, N. R. G., & Toucanne, S. (2015). An optimized scheme of lettered marine isotope substages for the last 1.0 million years, and the climatostratigraphic nature of isotope stages and substages. *Quaternary Science Reviews*, *111*(C), 94–106. https://doi.org/10.1016/j.quascirev.2015.01.012

Roberts, N. L., Piotrowski, A. M., McManus, J. F., & Keigwin, L. D. (2010). Synchronous deglacial overturning and water mass source changes. *Science*, *327*(5961), 75–78. https://doi.org/10.1126/science.1178068

Robinson, S., Ivanovic, R., van de Flierdt, T., Blanchet, C. L., Tachikawa, K., Martin, E. E., et al. (2021). Global continental and marine detrital εNd: An updated compilation for use in understanding marine Nd cycling. *Chemical Geology*, *567*, 120119. https://doi.org/10.1016/j.chemgeo.2021.120119

Schlitzer, R. (2021). *Ocean data view*. https://odv.awi.de

Schlitzer, R., Anderson, R. F., Dodas, E. M., Lohan, M., Geibert, W., Tagliabue, A., et al. (2018). The GEOTRACES Intermediate Data Product 2017. *Chemical Geology*, *493*, 210–223. https://doi.org/10.1016/j.chemgeo.2018.05.040

Shimizu, H., Tachikawa, K., Masuda, A., & Nozaki, Y. (1994). Cerium and neodymium isotope ratios and REE patterns in seawater from the North Pacific Ocean. *Geochimica et Cosmochimica Acta*, *58*(1), 323–333. https://doi.org/10.1016/0016-7037(94)90467-7

Stichel, T., Frank, M., Rickli, J., Hathorne, E. C., Haley, B. A., Jeandel, C., & Pradoux, C. (2012). Sources and input mechanisms of hafnium and neodymium in surface waters of the Atlantic sector of the Southern Ocean. *Geochimica et Cosmochimica Acta*, *94*, 1–50. https://doi.org/10.1016/j.gca.2012.07.005

Stramma, L., & England, M. H. (1999). On the water masses and mean circulation of the South Atlantic Ocean. *Journal of Geophysical Research*, *104*(20), 863–20. https://doi.org/10.1029/1999jc900139

Sun, S., Eisenman, I., & Stewart, A. L. (2018). Does southern ocean surface forcing shape the global ocean overturning circulation? *Geophysical Research Letters*, *45*(5), 2413–2423. https://doi.org/10.1002/2017gl076437

Talley, L. (2013). Closure of the global overturning circulation through the Indian, Pacific, and Southern Oceans: Schematics and transports. *Oceanography*, *26*(1), 80–97. https://doi.org/10.5670/oceanog.2013.07

Tanaka, T., Togashi, S., Kamioka, H., Amakawa, H., Kagami, H., Hamamoto, T., et al. (2000). JNdi-1: A neodymium isotopic reference in consistency with LaJolla neodymium. *Chemical Geology*, *168*(3–4), 279–281. https://doi.org/10.1016/s0009-2541(00)00198-4

van de Flierdt, T., Griffiths, A. M., Lambelet, M., Little, S. H., Stichel, T., & Wilson, D. J. (2016). Neodymium in the oceans: A global database, a regional comparison and implications for palaeoceanographic research. *Philosophical Transactions of the Royal Society A: Mathematical, Physical & Engineering Sciences*, *374*, 20150293. https://doi.org/10.1098/rsta.2015.0293

van de Flierdt, T., Robinson, L. F., Adkins, J. F., Hemming, S. R., & Goldstein, S. L. (2006). Temporal stability of the neodymium isotope signature of the Holocene to glacial North Atlantic. *Paleoceanography*, *21*, PA4102. https://doi.org/10.1029/2006pa001294

Vance, D., Scrivner, A., Beney, P., Staubwasser, M., Henderson, G. M., & Slowey, N. (2004). The use of foraminifera as a record of the past neodymium isotope composition of seawater. *Paleoceanography*, *19*(2), PA2009. https://doi.org/10.1029/2003pa000957

Wolff, E. W., Fischer, H., Fundel, F., Ruth, U., Twarloh, B., Littot, G. C., et al. (2006). Southern Ocean sea-ice extent, productivity and iron flux over the past eight glacial cycles. *Nature*, *440*(7083), 491–496. https://doi.org/10.1038/nature04614

Wu, Y. (2019). *Investigating the applications of neodymium isotopic compositions and rare Earth Elements as water mass Tracersin the South Atlantic and North Pacific*.

Yu, J., Menviel, L., Jin, Z. D., Anderson, R. F., Jian, Z., Piotrowski, A. M., et al. (2020). Last glacial atmospheric CO_2 decline due to widespread Pacific deep-water expansion. *Nature Geoscience*, *13*. https://doi.org/10.1038/s41561-020-0610-5

Zhao, N., Oppo, D. W., Huang, K.-F., Howe, J. N. W., Blusztajn, J., & Keigwin, L. D. (2019). Glacial-interglacial Nd isotope variability of North Atlantic Deep Water modulated by North American ice sheet. *Nature Communications*, *1*. https://doi.org/10.1038/s41467-019-13707-z

Ziegler, M., Diz, P., Hall, I. R., & Zahn, R. (2013). Millennial-scale changes in atmospheric CO_2 levels linked to the Southern Ocean carbon isotope gradient and dust flux. *Nature Geoscience*, *6*(6), 457–461. https://doi.org/10.1038/ngeo1782

Zimmermann, B., Porcelli, D., Frank, M., Rickli, J., Lee, D.-C., & Halliday, A. N. (2009). The hafnium isotope composition of Pacific Ocean water. *Geochimica et Cosmochimica Acta*, *73*(1), 91–101. https://doi.org/10.1016/j.gca.2008.09.033